Spatial Correlation Between Hα Emission and Infrared Cirrus

A. Kogut[1,2]

Accepted for publication by *The Astronomical Journal*
June 17, 1997

ABSTRACT

Cross-correlation of the DIRBE 100 μm survey with previously published Hα maps tests correlations between far-infrared dust and the warm ionized interstellar medium in different regions of the sky. A $10^\circ \times 12^\circ$ patch at Galactic latitude $b = -21^\circ$ shows a correlation slope $a_0 = 0.85 \pm 0.44$ Rayleighs MJy^{-1} sr significant at 97% confidence. A set of Hα images over the north celestial polar cap yields a weaker correlation slope $a_0 = 0.34 \pm 0.33$ Rayleighs MJy^{-1} sr. Combined with observations from microwave anisotropy experiments, the data show roughly similar correlations on angular scales $0.^\circ 7$ to 90°. Microwave experiments may observe more emission per unit dust emission than are traced by the same structures observed in Hα.

[1] Hughes STX Corporation, Laboratory for Astronomy and Solar Physics, Code 685, NASA/GSFC, Greenbelt MD 20771.
[2] E-mail: kogut@stars.gsfc.nasa.gov.

1 Introduction

Observations of anisotropy in the cosmic microwave background are complicated by the presence of foreground Galactic emission along all lines of sight. At high latitudes ($|b| > 10°$), diffuse Galactic emission is dominated by optically thin synchrotron, dust, and free-free emission. In principle, these components may be distinguished by their different spatial morphology and frequency dependence. In practice, there is no emission component for which both the frequency dependence and spatial distribution are well determined. Synchrotron radiation dominates radio-frequency surveys, but the spectral index steepens with frequency and has poorly-determined spatial variation (Bennett et al. 1992, Banday & Wolfendale 1991). Dust emission dominates far-infrared surveys, but its spectral behavior at longer wavelengths depends on the shape, composition, and size distribution of the dust grains, which are poorly known (Désert, Boulanger, & Puget 1990). Free-free emission from electron-ion interactions has well-determined spectral behavior but lacks an obvious template map: free-free emission never dominates the high-latitude radio sky, while other tracers of the warm ionized interstellar medium (WIM) such as Hα emission, pulsar dispersion measure, or N II emission are either incomplete, undersampled, or noise-dominated (Bennett et al. 1992, Reynolds 1992, Bennett et al. 1994).

The problem is particularly acute for free-free emission: lacking an accurate template for the spatial distribution, estimation of free-free emission requires pixel-by-pixel frequency decomposition which significantly reduces the signal to noise ratio of the desired cosmological signal. Recently, Kogut et al. 1996a proposed using infrared emission from diffuse cirrus as a tracer of the diffuse ionized gas responsible for free-free emission. Cross-correlation of the COBE Differential Microwave Radiometer (DMR) maps at 31.5, 53, and 90 GHz with the Diffuse Infrared Background Experiment (DIRBE) far-infrared maps at 100, 140, and 240 μm shows statistically significant emission in each microwave map whose spatial distribution on angular scales above 7° is traced by the far-infrared dust emission (Kogut et al. 1996b). The frequency dependence of this emission, rising sharply at long wavelengths, is inconsistent with the expected microwave dust emission. A 2-component fit to dust plus radio emission,

$$I_\nu \;=\; A_{\rm dust}\left(\frac{\nu}{\nu_0}\right)^{\beta_{\rm dust}} B_\nu(T_{\rm dust}) \;+\; A_{\rm radio}\left(\frac{\nu}{\nu_0}\right)^{\beta_{\rm radio}}$$

with $1.5 < \beta_{\rm dust} < 2$ yields spectral index $\beta_{\rm radio} = -0.3^{+1.3}_{-3.8}$ for the unknown component, strongly suggestive of free-free emission ($\beta_{\rm ff} = -0.15$). At high latitudes ($|b| > 20°$), spatial fluctuations in the diffuse synchrotron emission are uncorrelated with dust emission, leaving free-free emission (thermal bremsstrahlung) from the WIM as the only plausible alternative: on large angular scales, at least 30% of microwave emission from the WIM is traced by the diffuse infrared cirrus (Kogut et al. 1996b).

The detection of correlation between dust and ionized gas at high latitudes is consistent with the correlation observed between dust and free-free emission along the Galactic plane (Broadbent, Haslam, & Osborne 1989). Two questions of interest for cosmological observations are the extent to which infrared dust reliably traces high-latitude radio emission, and whether the correlation depends significantly on angular scale. Hα emission is a widely used tracer of the WIM. Recently, McCullough 1997 demonstrated a correlation between Hα emission and the IRAS infrared cirrus at 1° angular scale, with an amplitude comparable to the value derived from DMR at much larger angular scales. In this paper, I present results from cross-correlations of high-latitude Hα maps with the DIRBE 100 μm intensity on angular scales $0\overset{\circ}{.}7$ to 10°.

2 Analysis

If Hα emission is correlated with far-infrared dust, the Hα intensity in each pixel may be written as

$$H_i = aD_i + n_i, \tag{1}$$

where H is the intensity in the Hα map, D is the far-infrared intensity in the dust map, n represents an uncorrelated component (noise, systematic artifacts, or uncorrelated emission features), and i is a pixel index. The presence of correlation between two data sets is often quantified using the Pearson correlation coefficient,

$$\rho = \frac{\sum_i (D_i - \langle D_i \rangle)(H_i - \langle H_i \rangle)}{\left(\sum_i (D_i - \langle D_i \rangle)^2 \sum_i (H_i - \langle H_i \rangle)^2\right)^{1/2}}.$$

While this has the advantage of being a simple, dimensionless quantity that does not require detailed knowledge of noise or artifacts in the two data sets, it can not show whether the physically more interesting correlation slope a varies between different data sets at different locations or angular scales. An alternative approach uses the correlation slope a, defined as

$$a = \frac{\sum_{i,j} H_i (\mathbf{M}^{-1})_{ij} D_j}{\sum_{i,j} D_i (\mathbf{M}^{-1})_{ij} D_j} \tag{2}$$

with statistical uncertainty

$$\delta a = \left[\sum_{i,j} D_i (\mathbf{M}^{-1})_{ij} D_j \right]^{-1/2},$$

where $\mathbf{M}$ is the covariance matrix for emission between pixels i and j in the Hα map. In the limit $\mathbf{M}_{ij} = \sigma^2 \delta_{ij}$, where σ is the instrumental noise, equation 2 reduces

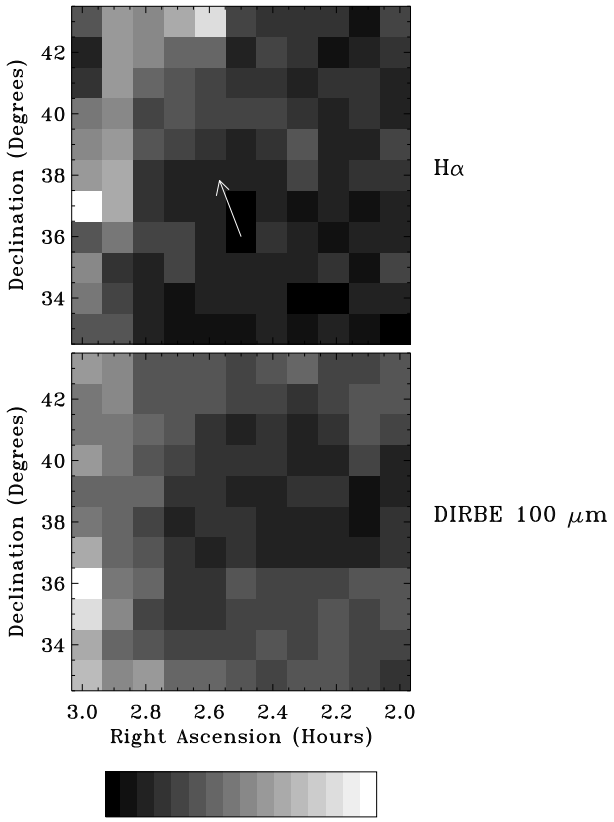

Figure 1: Reynolds 1980 Hα map and DIRBE 100 μm map in same sparse sampling. Full scale is 1–12 Rayleighs in Hα and 3.7–10.3 MJy sr^{-1} for DIRBE, with white regions brighter for both maps. The arrow shows the direction of lower Galactic latitude.

to a least-squares fit. Note that for totally uncorrelated maps $\langle HD \rangle = 0$ averaged over many pixels (or many maps), so that $\langle a \rangle = 0$ as expected when no correlation is present. Equation 2 has the additional desirable property of a well-defined distribution: given two uncorrelated data sets x and y with unit normal distribution, the distribution $a/\delta a$ will also have zero mean and unit standard deviation. The presence of a true correlation slope a_0 in the parent population shifts the mean fitted value $\langle a \rangle = a_0$ but does not alter the width of the distribution.

Few measurements of diffuse Hα emission exist at high Galactic latitude. Figure 1 shows the Hα intensity within a $10^\circ \times 12^\circ$ patch at $(l, b) = (144, -21)$

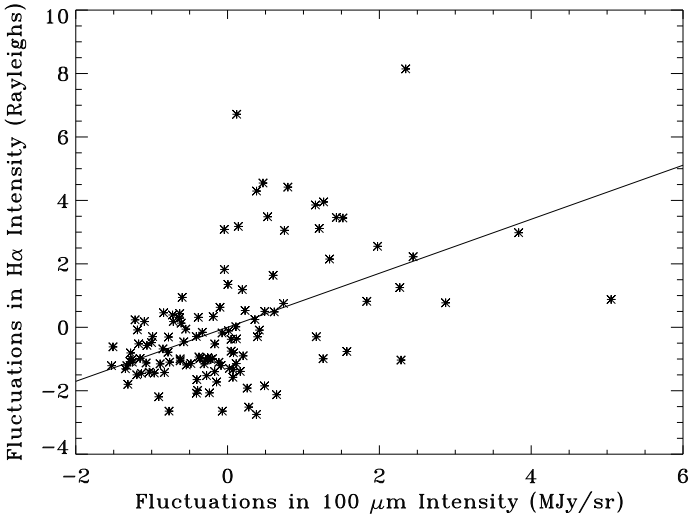

Figure 2: Reynolds 1980 Hα map and DIRBE 100 μm map plotted point by point. The fitted slope $a_0 = 0.85$ Rayleighs MJy^{-1} sr.

measured by a Fabry-Perot spectrometer with a 0.°8 beam sampled on a 1° grid (Reynolds 1980). The 100 μm emission measured by DIRBE at 0.°7 angular resolution is shown in the same sparse sampling. [1] Figure 2 plots the two maps point by point and shows the fitted correlation slope a for uniform pixel weight. Quantification of the correlation slope between the two data sets suffers from two problems. Uncertainties in the subtraction of geocoronal emission can contribute systematic artifacts comparable to the instrumental noise in each line of sight (Reynolds 1980). The small number of independent pixels (121) creates appreciable sample variance. The far-IR dust emission has a steep power spectrum, $P \propto \ell^{-3}$ where $\ell \propto \theta^{-1}$ is the spherical harmonic order (Gautier et al. 1992, Kogut et al. 1996a). Gradients in the Hα map may thus correlate with large-scale features in the far-IR dust emission simply by chance alignment.

These problems may be addressed using Monte Carlo techniques, repeating the fit in equation 2 after replacing the DIRBE patch $I_{\rm DIRBE}$ with a set of "control" patches selected from distant portions of the sky. Since the same Hα map is used for all trials, the distribution of fitted slopes automatically accounts for instrumental noise, systematic artifacts, and chance alignment, and provides a simple, robust description of the probability for an uncorrelated patch of cirrus to produce a slope a as large

[1] Throughout this paper I use the 100 μm map for its high signal to noise ratio and to facilitate comparison with the IRAS 100 μm survey at finer angular scales. I obtain similar results using the DIRBE 140 μm and 240 μm surveys.

(or larger) than the value from the correct part of the sky. Note that Eq. 2 is only asymptotically unbiased: although the Monte Carlo technique correctly accounts for the width of the distribution in a, instrumental noise in the "template" DIRBE map reduces the mean value by a factor $S^2/(S^2+n^2)$, where S and n are the signal and noise in the DIRBE map. For the data in this paper, $S/n \gg 1$ and the correction is negligible (less than 1%).

Far-IR emission is markedly anisotropic, so I restrict the control patches to those lying within the latitude range of the Hα map. For computational ease, I center each control patch on the pixel centers of the COBE quadrilateralized sky cube at resolution index 4 within the range $15^\circ < |b| < 30^\circ$, resulting in 64 independent cross-correlations. To allow for possible correlated csc(b) emission (with no smaller-scale correlations), I determine the distribution of fitted slope a with the control patches in random orientation with respect to the Hα map, and again with the control patches fixed with respect to the Galactic plane.

Figure 3 shows the distribution of the fitted correlation slopes a between the Reynolds Hα map and the set of randomly oriented control patches. The correlation slope a_0 between the Hα map and the DIRBE 100 μm map in the correct position is also shown. Only 3% of the uncorrelated control fields had $a > a_0$, suggesting a marginal detection of correlated emission between Hα and 100 μm dust, $a_0 = 0.85 \pm 0.44$ Rayleighs MJy^{-1} sr within the Reynolds field. Fixing

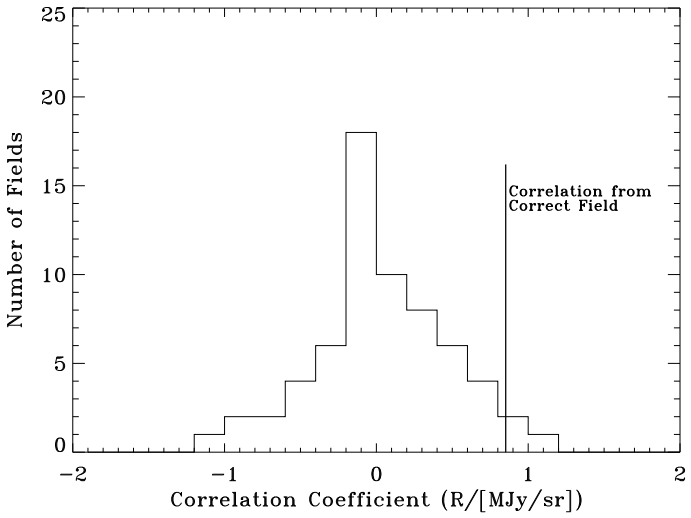

Figure 3: Histogram of fitted correlation slope between the Reynolds 1980 Hα map and a set of 64 DIRBE "control" fields. The correlation a_0 between the Hα map and the DIRBE intensity along the same lines of sight is also shown.

the orientation of the control patches with respect to the Galactic plane does not appreciably alter the results: the distribution of control patches still has zero mean and similar width, demonstrating that the observed correlation is not purely an artifact of general $\csc(b)$ trends in both data sets. Repeating the analysis with the Pearson correlation coefficient ρ instead of the correlation slope a provides similar, slightly more significant, results: $\rho = 0.48 \pm 0.22$, significant at 98% confidence.

Gaustad, McCullough, & Van Buren 1996 measured Hα emission at $0\overset{\circ}{.}1$ angular resolution using narrow-band CCD images in a series of $7^\circ \times 7^\circ$ fields covering

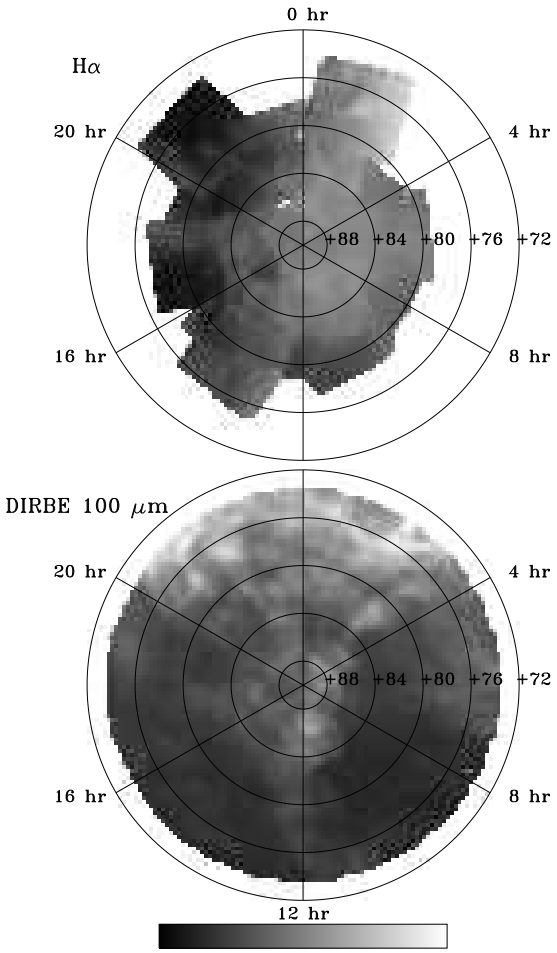

Figure 4: Hα mosaic over north celestial pole (Gaustad et al. 1996) and fluctuations in DIRBE 100 μm intensity. A mean has been removed from each data set. White is brighter for both maps.

the north celestial polar cap (declination $\delta > 81°$). Visible structure within the Hα fields is dominated by systematic artifacts (ghosts and stellar residuals), with intrinsic anisotropy less than 1.3 Rayleighs (Gaustad, McCullough, & Van Buren 1996). To reduce systematic artifacts, I reject all pixels in each field lying more than 3 standard deviations from the mean in that field, and then re-bin the remaining data into DIRBE pixels. Figure 4 shows a mosaic of the re-binned Hα map, along with the DIRBE 100 μm data.

Artifacts associated with field edges are evident in the Hα mosaic, and direct field to field comparison in regions where 2 or more fields overlap confirms that much of the large-scale structure is systematic in origin. Since power in the far-IR emission also increases on larger angular scales, the presence of large-scale systematics may be partially offset by increased sensitivity to diffuse structure in the DIRBE maps. To allow for this possibility, I cross-correlate the Gaustad et al. Hα data against the DIRBE data using two techniques. The first method simply correlates the full Hα mosaic with the DIRBE 100 μm map, using a set of control fields at $20° < |b| < 33°$ to estimate the uncertainty. The full mosaic shows no statistically significant correlation: 28% of the control fields had a correlation slope larger than the actual fields in the correct orientation, $a_0 = 0.21 \pm 0.43$ Rayleighs MJy^{-1} sr.

The correlation from the full mosaic is dominated by systematic artifacts at the field edges. A second method avoids these artifacts by correlating each of the sixteen $7° \times 7°$ fields independently, then using the arithmetic mean of the 16 fitted correlation slopes a_i to estimate the mean correlation over the full polar cap. As before, a set of control fields provides an estimate for the uncertainty in the mean correlation. 17% of the control fields had mean correlation larger than the actual fields in the correct orientation, yielding a correlation $a_0 = 0.34 \pm 0.33$ Rayleighs MJy^{-1} sr on angular scales $0.^\circ7$–$7°$ within the north celestial polar cap. The results do not change appreciably if the control patches are held in fixed orientation with respect to the Galactic plane.

3 Discussion

Figure 5 plots the correlation slope between the WIM and 100 μm dust emission as a function of angular scale. Since the dust power spectrum varies as θ^3, the data are shown at the largest angular scale probed by each experiment. Data from microwave experiments (DMR:Kogut et al. 1996b; Saskatoon:de Oliveira-Costa et al. 1997) are expressed in Rayleighs assuming a spectral index $\beta_{\rm ff} = -0.15$ and a conversion 2 μK/Rayleigh at 53 GHz appropriate for gas at 8000 K. There is no compelling evidence for variation in the correlation slope as a function of angular

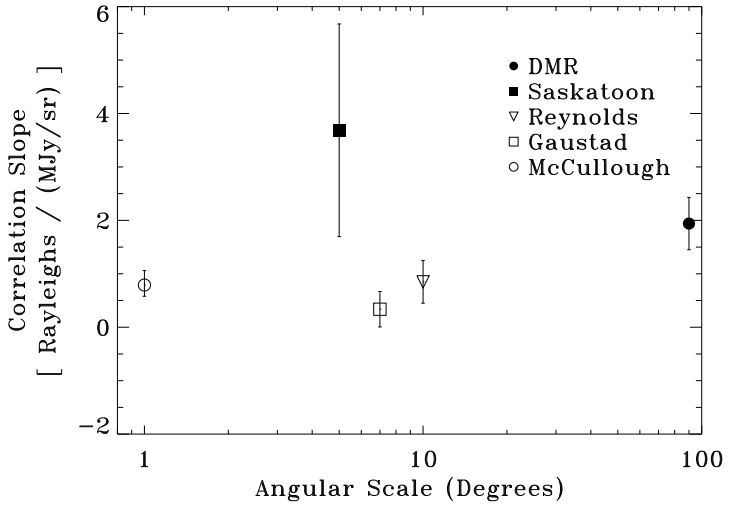

Figure 5: Correlation slopes a between the warm ionized interstellar medium and far-infrared dust emission as a function of largest angle probed by each experiment. Open symbols refer to Hα data and filled symbols refer to microwave measurements. DMR: Kogut et al. 1996b; Saskatoon: de Oliveira-Costa et al. 1997; McCullough: McCullough 1997; all others:this work.

scale.

The limited data in Figure 5 appear to fall in two groups, with correlations derived from microwave observations lying higher than direct Hα correlations, even in the NCP field where both microwave and Hα data are available. Although the uncertainties on any individual measurement are appreciable, the mean slope derived from microwave observations lies 2.7 standard deviations above the mean of the three direct Hα observations. Both observations detect structure correlated with the spatial distribution of the infrared cirrus, but the microwave experiments appear to observe more emission per unit dust than are traced in Hα.

Further evidence for "extra" microwave emission traced by the infrared cirrus comes from the MAX5 microwave anisotropy experiment (Lim et al. 1996). Data from the MAX5 experiment show statistically significant correlations between the IRAS 100 μm map and millimeter-wavelength anisotropy measurements centered at at 105, 180, 270, and 420 GHz. The frequency dependence is consistent with a superposition of dust plus a second component identified as either free-free emission or anisotropy in the cosmic microwave background; although free-free emission is preferred, the data do not distinguish decisively between these alternatives. The amplitude of the second component is large: if it results from free-free emission, the implied correlation slope

between the WIM and dust is $a = 37 \pm 19$ Rayleighs MJy^{-1} sr on angular scales $\theta \approx 2^\circ$ within the MAX5 μ Pegasi field (Lim et al. 1996). Such a result would imply even greater variation in WIM/dust correlation than already evident in Figure 5 (since the MAX5 result can not be attributed definitively to Galactic emission, it is not plotted). Variation in the electron temperature within the WIM would change the ratio of microwave free-free emission to Hα emission. However, the temperature of the high-latitude cirrus (presumably heated by the same interstellar radiation field as the WIM) is constant within 10% when averaged over broad regions (Reach et al. 1995), making problematic any preferential heating of the WIM. Other possible emission mechanisms that would produce long-wavelength emission correlated with emission from the IR cirrus include flat-spectrum synchrotron from supernovae shock fronts and radio emission from rotating charged dust in the WIM (Ferrara & Dettmar 1994).

4 Summary

Cross-correlation of the DIRBE 100 μm survey with previously published Hα maps yields positive correlation with amplitude comparable to previously published Hα and microwave results. The combined data show no dependence on angular scale, indicating that existing infrared maps can be used to trace microwave emission over scales $0\overset{\circ}{.}7$ to 90°. Microwave experiments show a marginally significant trend toward observing more microwave emission per unit dust emission than are traced by the same structures observed in Hα. Additional observations, both Hα and microwave, are required to determine if this results from a statistical fluke, variations within the WIM, or the existence of competing emission mechanisms traced by the spatial distribution of high-latitude dust.

Gary Hinshaw provided helpful conversations. This work was supported in part by NASA RTOP 399-20-61-01.

References

Banday, A. & Wolfendale, A.W. 1991, MNRAS, 248, 705
Bennett, C.L., et al. 1992, ApJ, 396, L7
Bennett, C.L., et al. 1994, ApJ, 434, 587
Broadbent, A., Haslam, C.G.T., & Osborne, J.L. 1989, MNRAS, 237, 381
de Oliveira-Costa, A., et al. 1997, ApJ, 482, L17
Désert, F.-X., Boulanger, F., & Puget, J.-L. 1990, A&A, 327, 215
Ferrara, A., & Dettmar, R.-J. 1994, ApJ, 427, 155
Gaustad, J.E., McCullough, P.P, & Van Buren, D. 1996, PASP, 108, 351
Gautier, T.N., Boulanger, F., Pérault, M., & Puget, J.L. 1992, AJ, 103, 1313
Kogut, A., et al. 1996a, ApJ, 460, 1
Kogut, A., et al. 1996b, ApJ, 464, L5
Lim, M.A., et al. 1996, ApJ, 469, L69
McCullough, P.R. 1997, AJ, 113, 2186
Reach, W.T., et al. 1995, ApJ, 451, 188
Reynolds, R.J. 1980, ApJ, 236, 153
Reynolds, R.J. 1992, ApJ, 392, L35